X-ray Diffraction Measurements of Laser-Generated Plasmas

Deshpreet Singh Bedi
University of Rochester, Laboratory for Laser Energetics
2006 Summer High School Program

ABSTRACT

Plasmas generated by the implosion of targets by the OMEGA laser emit x rays. Diffraction gratings can spatially separate the different wavelengths of these x rays. Measurement of the resultant space-resolved, continuum x-ray emission spectrum can provide valuable information regarding the properties of the plasma, such as core temperature, surface flux density, and source size.

The plasma, however, has a spatial distribution which blurs the diffracted spectrum, especially near the high energy end. This blurring can be described by a mathematical operation called a convolution. To accurately measure parameters of the plasma in the presence of spatial blurring, the effect on the grating-dispersed spectrum must be taken into account. The method used in this work is to take a spectral shape such as an exponential, a shape expected from a hot plasma, or the spectrum predicted by simulation, include the instrument efficiency, and compute the grating-dispersed spectrum. This is then convolved with a Gaussian spatial distribution, producing a mathematical model of the observed spectrum. A best fit of this model to the measurements yields estimates of the plasma parameters.

INTRODUCTION

The OMEGA laser facility[1] at the University of Rochester's Laboratory for Laser Energetics is currently being used to pursue the goal of obtaining thermonuclear ignition in the laboratory. Thermonuclear ignition requires both high temperature ($\geq$ 10 keV) and high density ($\geq$ 100 g/cm^3) conditions to exist in the plasma. The OMEGA laser facility is used to approach

these conditions, through the implosions of targets such as cryogenic deuterium-tritium (DT)-filled shells.[2] These shells become plasmas with central temperatures and densities comparable to those existing in the sun's interior (the sun's interior has a temperature of ~1.4 keV and a density of ~150 g/cm^3).[3] In the laser-generated plasma, the goal is to achieve much higher temperatures with more highly reactive fuel (DT) since, unlike the sun, the laboratory plasma exists in the hot dense phase for only about 10^{-10} seconds before expanding rapidly. In contrast, the sun is believed to burn its fuel for billions of years (~10^{17} sec).

The imploded interiors of the plasmas emit x rays.[4] X rays range from wavelengths of 100 Å (soft) to 0.01 Å (hard) (1 Å=10^{-10} m).[5] X rays emitted from the core plasma are differentially absorbed by the cooler surrounding shell of plasma, with absorption a strong function of energy.[4] The soft x rays are absorbed more strongly than the hard x rays. The x rays are imaged by a Kirkpatrick-Baez (KB) microscope[6] in the experiments reported here. The x rays also pass through a diffraction grating, made at LLE by a process including photolithography and reactive ion etching.[7] The emitted x rays are dispersed by wavelength upon passing through the diffraction grating. The diffracted images are recorded either by the time-integrated exposure of Kodak Biomax-MS film or by the absorption of photons by a solid-state, charge-injection device (CID).[8] Measuring the resultant broadband continuum spectrum provides information about the compressed shell temperature and the areal density of the plasma.[4]

The finite size of the laser-generated plasma results in a spectrum of x rays after diffraction that is not completely separated by wavelength and is blurred by the spatial distribution of the source [Fig. 8(a)]. In this report, a method of accounting for the effect of spatial blurring on the determination of the plasma emission spectrum is described, the goal

being to accurately model the diffracted x-ray spectrum in order to best measure the plasma size, temperature, and density in the presence of this blurring.

METHOD

A. X ray Emission

X rays are produced when any electrically charged particle of sufficient kinetic energy decelerates. In the laboratory, x rays are produced by accelerating electrons emitted by a hot filament towards a metal target (anode).[9] When the electrons strike the anode, they eject inner shell electrons off the anode, leaving a vacancy. These vacancies are filled by subsequent electron transitions from higher shells to lower ones, which result in the emission of x rays. The energy of these emitted x rays is characteristic of the electron transitions, which are dependent on the anode metal.

The x rays emitted from the anode have been found to consist of a mixture of different wavelengths, creating a continuous radiation, or Bremsstrahlung. This continuous spectrum results from the fact that not every electron decelerates in the same way. Some release all their energy at once, with one impact when they encounter the atoms of the metal target, while others deflect randomly many times, losing a fraction of their energy each time. When the voltage across the electrodes is raised above a certain level characteristic of the metal target, however, the characteristic line emission described above is observed superimposed on the continuous spectrum. Where large amounts of continuous radiation are desired in the laboratory, a heavy metal like tungsten and as high a voltage as possible should be used.[10]

B. Diffraction Gratings and Dispersion

At its simplest, diffraction involves a monochromatic beam of electromagnetic radiation (i.e. light) emitted from a point source encountering a single slit. Light is composed of wave

fronts of certain wavelength, which, upon impinging on the slit, emanate from each point in the slit as if they were point sources. The result of diffraction is an interference pattern, or a cyclic distribution of bright and dark spots. Bright spots result where the wave fronts arrive in phase, while dark sports result where the wave fronts arrive 180° out of phase. Increasing the number of slits sharpens the principal maxima (bright spots).

An increased number of slits also increases dispersion when dealing with radiation of many different wavelengths. Diffraction gratings are used to disperse light by wavelength and x rays are no exception. The diffraction gratings used at LLE are transmission gratings with 5000 lines/mm (Fig. 1) and are exactly like those designed for the Chandra X-Ray Observatory[7] having been built at the same facility. The gold bars are nearly opaque to radiation, so principally the x rays that pass between the bars will be transmitted and diffracted.

The dispersion of x rays by wavelength is given by the grating equation[11]

$$n\lambda = d_g \sin\theta , \tag{1}$$

where n is the diffraction order number, λ is the wavelength, d_g is the grating spacing, and θ is the diffraction angle. Because the x-ray emission from a laser-generated plasma source is not composed of just one wavelength and because the plasma is not a point source (i.e. it has a spatial distribution), there are no distinct peaks of maximum intensities at the various orders of diffraction. Rather, there is a continuum spectrum of all the x-ray wavelengths emitted from the plasma source [Fig. 8(a)]. There is also a zeroth-order image, which consists of undiffracted x rays, but in this study, only the first orders of diffraction (on either side of the zeroth-order image) are considered. Since diffraction angles are small,

$$\sin\theta \approx \frac{x}{D_i} \tag{2}$$

where x is the distance from the zeroth order image and D_i is the distance from the grating to the image plane (Fig. 2).

Substituting for $sin\theta$ in the grating equation produces an equation relating position along the image plane (the x direction of Fig. 8) to the wavelengths of the diffracted x rays,

$$\lambda \approx \left(\frac{d_g}{D_i} \right) x \tag{3}$$

where d_g/D_i is the dispersion power of the grating (Å/mm). The lower this value is, the more dispersed the diffracted spectrum is. For this study, the dispersion power is 0.9404 Å/mm.

C. X-ray emission from a Plasma

X-ray emission from a plasma—whether a celestial source such as a supernova remnant[12] or the core of a laser-imploded shell target—differs from x-ray emission from the bombardment of a metal target with electrons. The emission from a hot, dense plasma has a spectrum that depends on the temperature of the plasma. Radiation from a plasma can be classified as continuous radiation, or Bremsstrahlung.[13] A model of this radiation spectrum is given by an exponential,

$$\frac{ds}{dE} = j_o \exp\left(- E \big/ kT \right), \tag{4}$$

where *ds/dE* is the surface emissivity of the target in keV/keV/cm^2, j_o is the surface energy flux density in keV/keV/cm^2, E is the energy of the x rays in keV, and kT is the core temperature of the target in keV.[13]

Since the KB microscope is used to obtain a magnified image of a portion of the laser-target emission, *ds/dE* is related to the flux detected at the image plane (*df/dE*) by[4]

$$\frac{df}{dE} = \frac{ds}{dE}\frac{\Delta\Omega}{4\pi}\frac{\varepsilon}{M^2}, \tag{5}$$

where $\Delta\Omega$ is the solid angle subtended by the microscope [equal to the cross-sectional area of the image detector divided by the square of the distance between the source and the detector], M is the magnification of the image (given by $M=D_i/D_s$), and ε is the throughput efficiency of the total system (a function of energy), given by,

$$\varepsilon(E) = \varepsilon_g(E)T_f(E) \tag{6a}$$

$$T_f(E) = e^{-\mu(E)\rho\Delta x}, \tag{6b}$$

where ε_g is the grating efficiency, T_f is the filter throughput efficiency, μ is the mass absorption coefficient of the filter in cm^2/g, ρ is the filter density in g/cm^3, and Δx is the thickness in cm of the filter, typically composed of beryllium.

What is observed after dispersion by the grating (but before consideration of the spatial distribution of the plasma), however, is a spectrum varying with respect to position—the differential dispersed flux *df/dx*, a measurement of fluence values with respect to position on the spectrum. *Df/dE* is related to *df/dx* through multiplication with the differential *dE*/dx. By using the relationship $E=hc/\lambda$ in Eq. (3) and differentiating both sides, it is found that

$$\frac{dE}{dx} = -\frac{E^2}{hc}\frac{d_g}{D_i}, \tag{7}$$

the negative sign arising from the fact that increasing energy is in the direction of decreasing position (i.e. dispersion distance). Finally, the observed differential dispersed flux *df/dx* can be related to the target surface flux density *ds/dE* with the relationship

$$\frac{df}{dx} = -\frac{ds}{dE}\frac{E^2}{hc}\frac{d_g}{D_i}\frac{\Delta\Omega}{4\pi}\frac{\varepsilon}{M^2}. \quad (8)$$

Because of the limited resolution of the imaging device, however, the flux *df* (keV/cm^2) cannot be measured for an infinitesimal length *dx*; flux detectors at the image plane have finite-sized bins (pixels) into which all the flux in that area is added together. What is inferred as the dispersed spectrum from a point source (i.e. before taking into account the spatial distribution of the plasma source) is *df*, which is Eq. (8) multiplied by *dx*, which can be expressed as a finite length, Δx.

D. Convolution of Space and Spectrum

The laser-generated plasma, which emits x rays, is not a point source. X rays passing through the diffraction grating are blurred spatially. The dispersed image is spectrally blurred, resulting in an averaging of fluence values in space. This blurring can be described by a mathematical operation called a convolution. The convolution of two-dimensional functions is given by

$$C(x,y) = g(x',y') \otimes h(x,x',y,y') = \int_{space} g(x',y')h(x-x',y-y')dx'dy' \quad (9),$$

and can be described as an integral of a product of shifted copies of one function (*h*) with another (*g*).

The observed dispersed spectrum is a convolution of space and spectrum, where the spectrum is shifted and weighted by the values of a spatial distribution. This observed dispersed spectrum can be modeled by applying the convolution operation to the ideal exponential spectrum, *df*, with a normalized Gaussian source distribution (total area is 1) given by

$$g(x,y) = \frac{1}{\pi\sigma^2} e^{-(x^2+y^2)/\sigma^2}, \qquad (10)$$

where σ is the standard deviation and calculated as ~0.6 times the full width at half maximum of the measured spectrum (allowing for the calculation of meaningful physical sizes for the spectrum and Gaussian distribution in relation to each other).

CALCULATIONS

The programming language PV-WAVE[14] was used to facilitate the modeling of a dispersed convolution. First, the program *xray_spec* was written to generate a simple model exponential spectrum *df* before consideration of the spatial blurring of the plasma. A sample computed dispersed spectrum is shown in Fig. 3 for selected values of source temperature, kT, and surface energy flux density, j_o [see Eq. (4)].

When the efficiency response of the diffraction grating and the filter transmission are included, the fluence values are reduced and features are added to the calculated flux density spectrum (Fig. 4), due to energy-dependent factors. Low-energy x rays (less than 2 keV, corresponding to dispersion positions greater than 6.6 mm on Figs. 3 and 4) were practically removed from the spectrum because of absorption in the beryllium filters (127 μm thick filter in this computation). The feature at 6 mm (corresponding to 2.2 keV) is due to a decrease in the diffraction efficiency of the gold bars in the diffraction grating.[4]

The program *gauss_gen* is used to generate a normalized two-dimensional Gaussian distribution [Eq. (10)], which is used to represent the spatial distribution of the plasma. Both the spectrum and Gaussian distribution are calculated on the same scale, corresponding to images with pixels of size 20 μm. This allows for an accurate convolution and dispersed spectrum that can be readily compared to grating dispersed images recorded on film. By entering a standard

deviation value σ as a parameter, a two-dimensional Gaussian of appropriate size is generated.

A lineout through the central pixel row of any of the convolved spectra, when compared to the point-source spectrum, shows the effects of convolution. The fluence values from a finite-sized plasma source are much lower than those from a point source (Fig. 5a), due to the fact that the blurring due to the spatial distribution has spread the energy flux density contained in one pixel over a width of many pixels. Adding up the values of fluence in a one-pixel-wide cross-section of the dispersed spectrum yields a result nearly equal to the fluence of the point-source spectrum at that same position. The minor loss can be accounted for by the spectral (horizontal) blurring (i.e. mixing of x rays of different energies). When compared on a normalized scale, it is clear that the features in the point-source spectrum due to the instrument responses have been blurred out, and the high-energy values (greater than 5 keV, corresponding to positions less than 2.6 mm) are greatly affected by the finite source size of the plasma (Fig. 5b).

MODELING OF EXPERIMENTAL SPECTRA

The spectra of dispersed x rays from two different cryogenic target implosions were modeled. Graphs of the spectral fluence (Figs. 6 and 7) , *dE/d(hv)* (*ds/dE* integrated over space), as a function of energy for OMEGA laser shots 44182 and 44602 allow for a straight line fit (in a semi-log plot) of a simple exponential to the measured data to be determined. The slope of the line is related to the source temperature, kT, by the relationship

$$kT = \frac{-(E_1 - E_2)}{\ln(I_1 / I_2)}, \tag{11}$$

where I_1 and I_2 are values of intensities in keV/keV at the energies E_1 and E_2, respectively. $I_{0,}$ the surface intensity, is determined algebraically once kT is known. Division by the pixel area (in cm^2) gives j_o, allowing for the calculation of space-resolved fluence. Each graph also contains

the LILAC-hydrocode-simulation predicted emission spectrum,[2] which takes into account absorption of the emitted lower-energy x rays by the cold outer fuel shell of the imploded plasma.

The dispersed x-ray spectra were computed using Eq. (8) from the surface fluence spectra for both the best-fit ideal exponential and the LILAC simulation, using a value of 3.63×10^{-9} steradians for the solid angle subtended by the microscope, 14.4 for the magnification, 0.9404 Å/mm for the dispersion constant, and 0.02 mm for the pixel size. Because the measured diffracted x-ray spectra are recorded on film, the spectra are measured in film density and have additional features due to the energy-dependent sensitivity of the film. In order to allow for the close approximation of the calculated spectra with the measured film spectrum, *df* was converted from units of keV/cm^2 to units of photons/μm^2, by dividing by the photon energy values (keV) and multiplying by 10^{-8} cm^2/μm^2. A more exact treatment will need to take into account the exact dependence of film density on x-ray exposure.[15,16]

In order to approximate the source size of the plasma used in calculating a Gaussian spatial distribution, a measurement of the full width at half maximum (FWHM) of the measured spectrum was made using PV-WAVE by creating a line-out through the width of the spectrum. A FWHM of 50 μm was measured, and using Eq. 10 a standard deviation of 30 μm was calculated for the Gaussian. The calculated spectra were then convolved with the 2-dimensional Gaussian using the CONVOL function in PV-WAVE.

For OMEGA shot 44182 (Fig. 8), both the ideal exponential and the LILAC spectrum show a dispersed spectrum with similar shape and size to that of the measured film-imaged spectrum. Though the ideal exponential did not take into account absorption of x rays below ~ 2 keV in the plasma and the LILAC simulation did, the two calculated spectra are almost identical,

due to the absorption of low-energy x rays by the beryllium filters. Both models, however, assume more absorption than what was measured, shown by the premature trailing off of the spectra in the direction of increasing x (i.e. decreasing energy).

For OMEGA shot 44602 (Fig. 9), while the ideal exponential still shows a similar shape and size to that of the measured spectrum, the LILAC simulation shows many differences. It calculates much more absorption than what was measured, and it assumed a hotter temperature for the plasma source, as seen by the closer proximity of the high-energy ends of the spectrum to the middle. This was to be expected, as the slope of the LILAC simulation in Fig. 7 deviated from the slope of the actual measurements and the ideal exponential.

CONCLUSION

Implosions of cryogenic fusion targets are diagnosed with a diagnostic that measures the spectrum of x rays from the hot, imploded core. Interpretation of the image data is complicated because it is affected by the spatial distribution of the x-ray emitting region. Accounting for the convolution of space and spectrum in the diffraction of x rays due to the plasma source not being a point source is important because the slope of the spectral fluence values is affected by the spatial distribution of the plasma, which affects the estimate of kT. In this investigation, a method for accurately modeling a measured x-ray spectrum has been introduced. Being able to model the spatially-dispersed spectrum allows for a minimization of differences between the measured and calculated spectra, enabling more accurate estimation of the plasma's core temperature and source size. Future work will improve on this optimization by converting the model spectra into film density so that the differences between the model and measured spectra are only due to the differences in plasma parameter values.

ACKNOWLEDGEMENTS

I would like to thank my advisor Dr. Frederick J. Marshall for all of his help, guidance, and support throughout this project. I would also like to thank Dr. Stephen Craxton for welcoming me into this program and the LLE staff for creating such a hospitable environment.

REFERENCES

1. T. R. Boehly, D. L. Brown, R. S. Craxton *et al.*, Opt. Commun. **133**, 495 (1997).

2. F. J. Marshall *et al*., Phys. Plasmas, **12**, 056302 (2005).

3. Cox, Arthur N., Allen's Astrophysical Quantities (Fourth Edition). (The Estate of C.W. Allen/Springer-Verlag New York, Inc.: New York, NY, 2000), pp. 342.

4. F. J. Marshall *et al.*, "Diagnosis of laser-target implosions by space-resolved continuum absorption x-ray spectroscopy," Phys. Rev. **49,** 49 (1994).

5. Cullity, B. D., Elements of X-Ray Diffraction (Third Edition). (Prentice-Hall, Inc.: Upper Saddle River, NJ, 2001), pp. 1-3.

6. P. Kirkpatrick and A. Baez, J. Opt. Soc. Am. **38**, 766 (1948).

7. C. R. Canizares *et al.*, "The High Energy Transmission Grating Spectrometer for AXAF," *SPIE: X-Ray Instrumentation in Astronomy* **597,** 253 (1985).

8. F. J. Marshall *et al.*, "Imaging of laser-plasma x-ray emission with charge-injection devices," Rev. Sci. Instrum. **72,** 713 (2001).

9. Cullity, ibid., pp. 4-19.

10. Cullity, ibid., pp. 5-7.

11. Halliday, D. and R. Resnick, Fundamentals of Physics. (John Wiley and sons: New York, NY, 1970), pp. 744-746.

12. K. A. Flanagan *et al.*, "*CHANDRA* high-resolution x-ray spectrum of supernova remnant 1E 0102.2-7219," *The Astrophysical Journal* **605,** 230 (2004).

13. Lang, K. R., Astrophysical Formulae, Volume 1: Radiation, Gas Processes and High Energy Astrophysics. (Springer-Verlag: New York, NY, 1999), pp. 48-49.

14. Visual Numerics, Inc. Houston, TX 77042

15. F. J. Marshall *et al.*, "Absolute calibration of Kodak Biomax-MS film response to x rays in the 1.5- to 8-keV energy range," Rev. Sci. Instrum. **77**, 10F308 (2006).

16. J. P. Knauer *et al*., Rev. Sci. Instrum. **77**, 10F331 (2006).

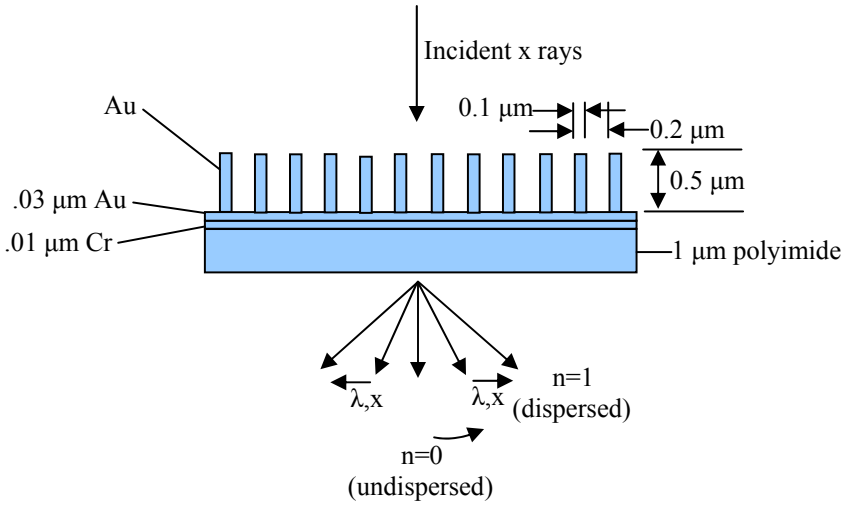

Fig. 1. Diagram of a transmission diffraction grating, showing undispersed (n=0) and dispersed (n=1) orders in the x direction.

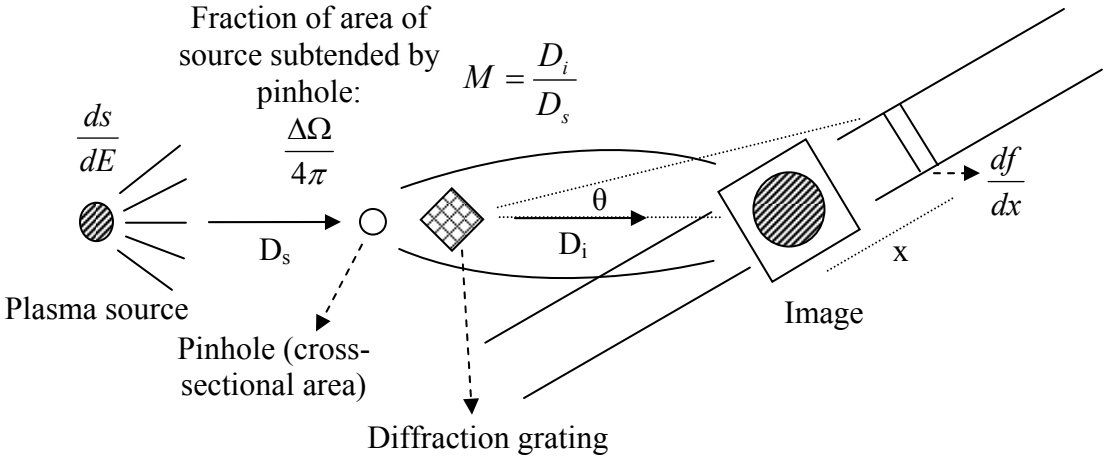

Fig. 2. Diagram of the imaging and diffraction of x rays emitted from a spatially-distributed plasma source. The image plane, shown schematically here, is perpendicular to the direction of x-ray propagation. For simplicity, the image is shown here as being formed by a pinhole rather than the functionally similar x-ray mirrors used by the KB microscope.

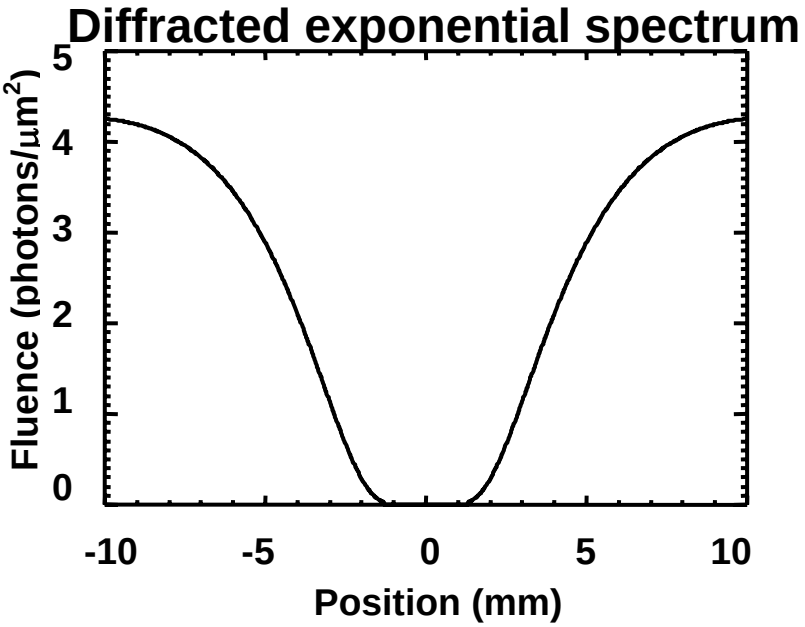

Fig. 3. An example of a dispersed exponential spectrum before consideration of the spatial blurring of the plasma. Position corresponds to the x direction of Fig. 8.

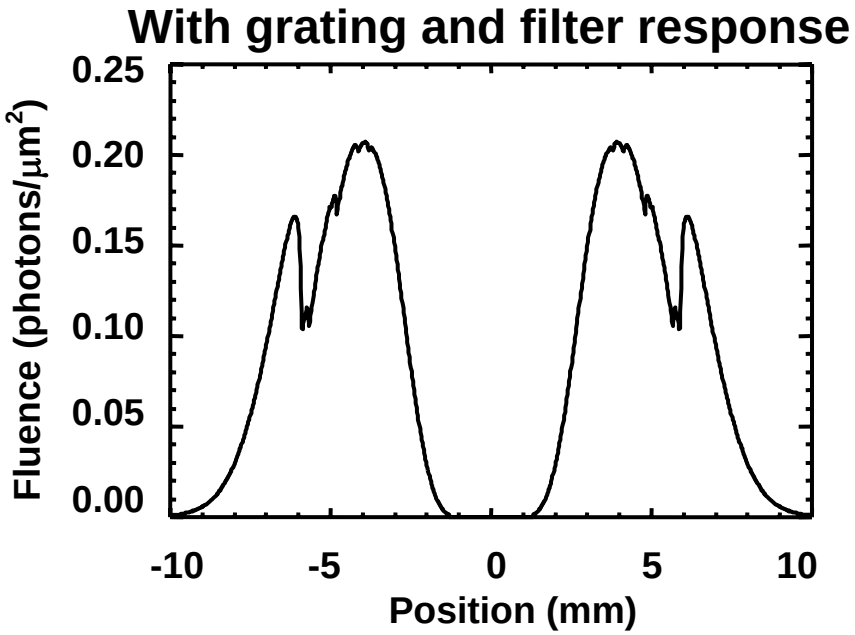

Fig. 4. The dispersed exponential spectrum of Fig. 3 after the addition of the efficiency response of the diffraction grating and the filter transmission.

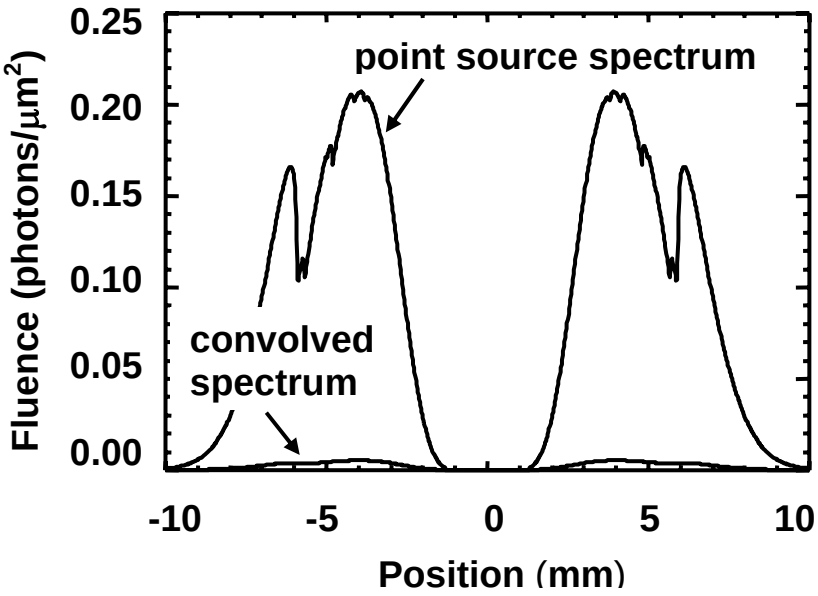

Fig. 5a. Comparison of the dispersed exponential spectra before and after consideration of the source's spatial distribution. The effect of having a finite-sized plasma source is to greatly reduce the fluence values contained in a line-out through the center row of the spectrum.

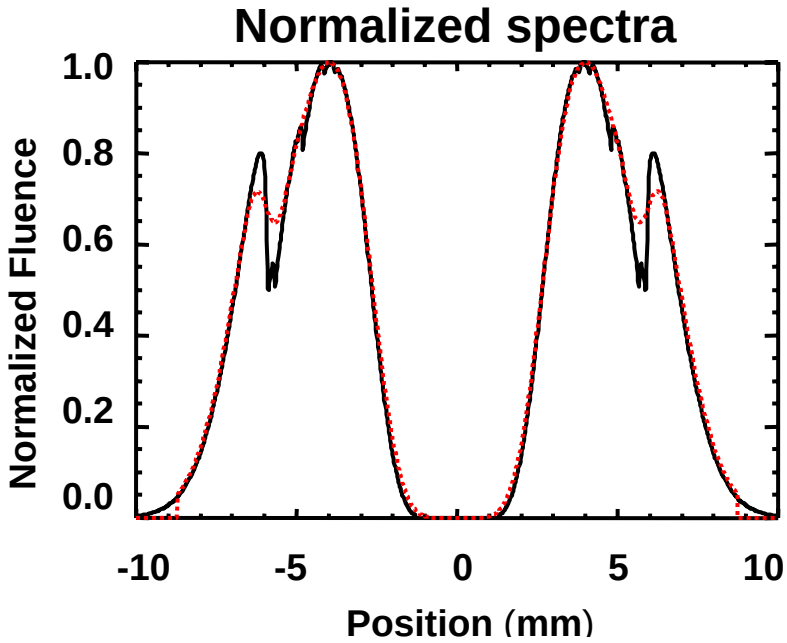

Fig. 5b. Same as Fig. 5a but with both spectra normalized. The red curve is the convolved spectrum. The effect of having a finite-sized source is also to blur out the features in the point-source spectrum due to the instrument responses.

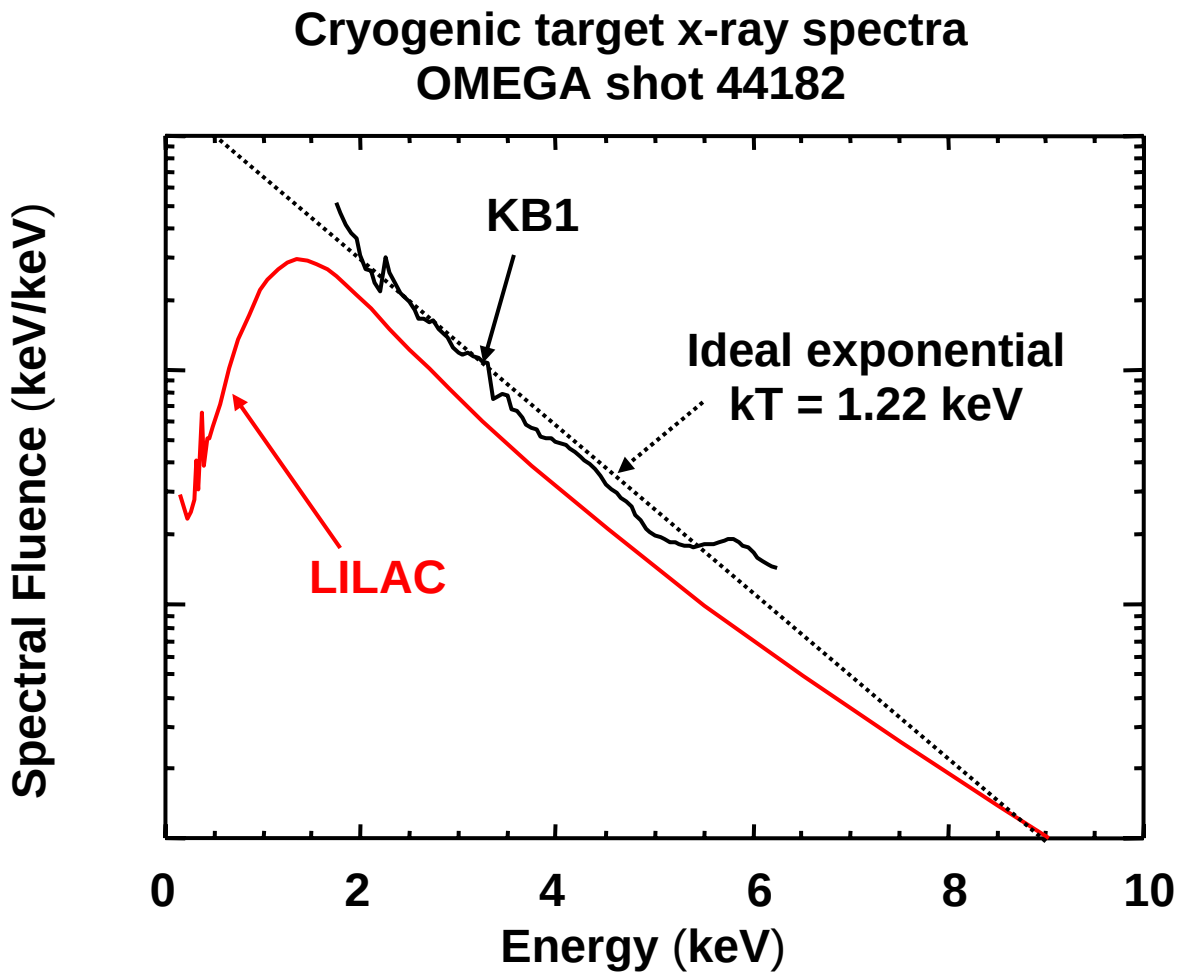

Fig. 6. Graphs of the spectral fluence, *dE/d(hv)* (*ds/dE* integrated over space), as a function of energy. The KB1 curve is determined directly from the imaged spectrum using the KB microscope, while the LILAC curve is a hydrocode simulation. Graphing in a semi-log plot allows for a straight line fit of a simple exponential to the measured data to be determined. The slope of the line is related to the source temperature, kT.

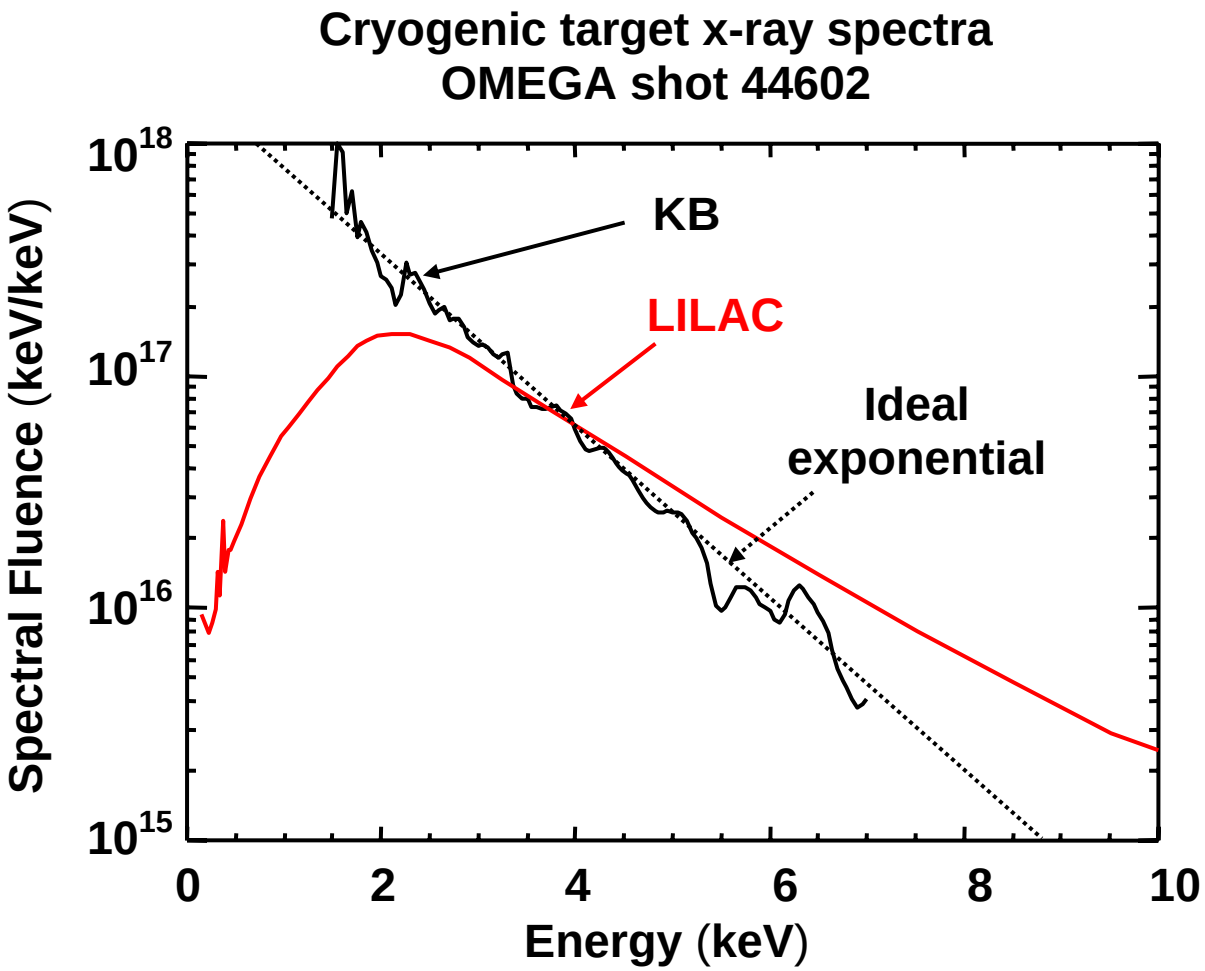

Fig. 7. Graphs of the measured, predicted, and exponentially-modeled spectral fluence of a second OMEGA laser shot.

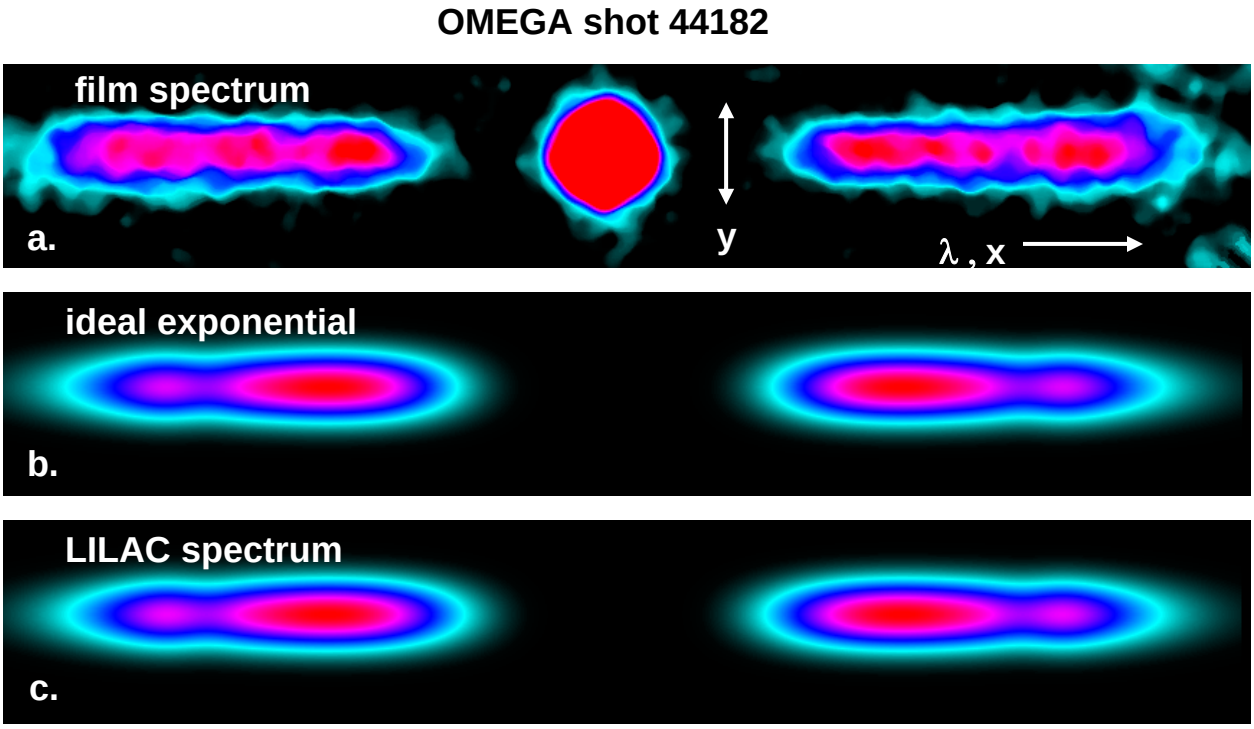

Fig. 8. Measured x-ray spectrum using a KB microscope (a), showing the zeroth and first diffraction orders. The finite size of the plasma source has blurred the first order spectra both spectrally (x direction) and spatially (y direction). Convolution of the x-ray flux *df*, determined from either given (LILAC) or calculated (exponential) spectral fluence values (Fig. 6), with a Gaussian source distribution results in model x-ray spectra (b & c) that can be compared with the imaged spectrum (a).

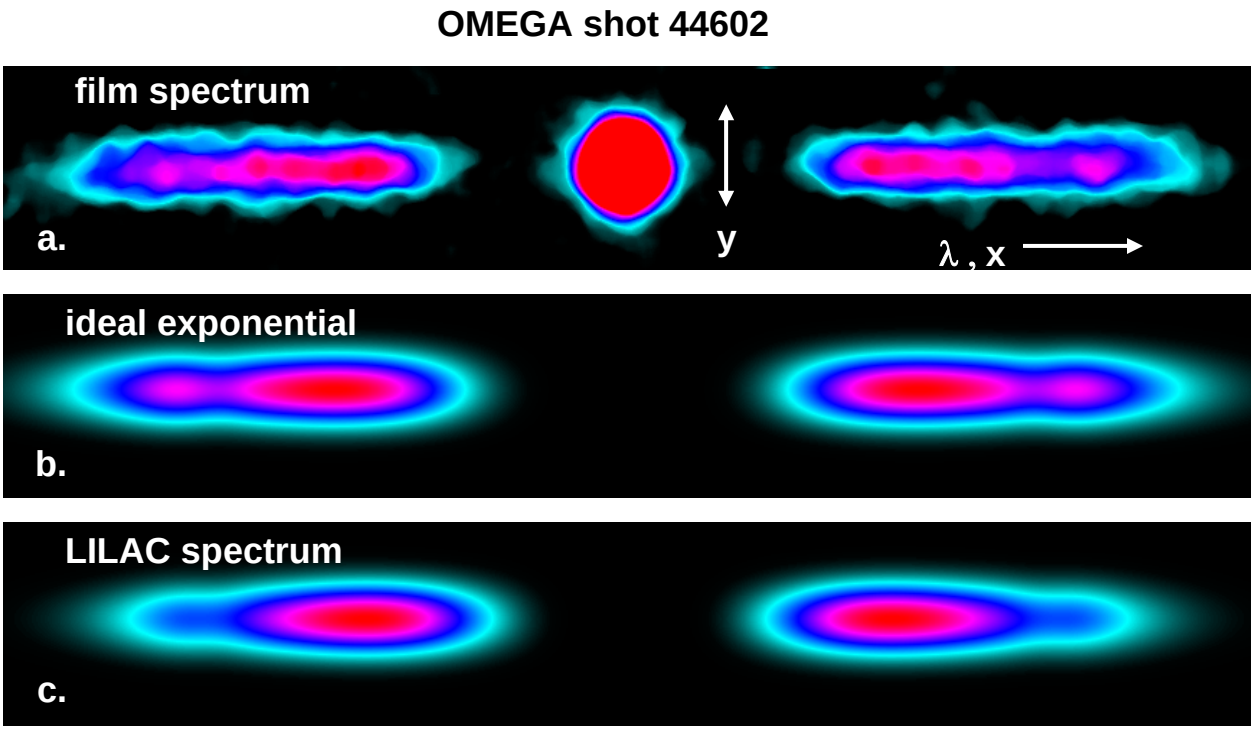

Fig. 9. Comparison of the convolved spectra from the spectral fluence values of Fig. 7 with the imaged spectrum for OMEGA laser shot 44602.